LAMINAR SOOT PROCESSES

P.B. Sunderland, K.-C. Lin, and G.M. Faeth
The University of Michigan
Ann Arbor, Michigan

Introduction

Soot processes within hydrocarbon fueled flames are important because they affect the durability and performance of propulsion systems, the hazards of unwanted fires, the pollutant and particulate emissions from combustion processes, and the potential for developing computational combustion. Motivated by these observations, the present investigation is studying soot processes in laminar diffusion and premixed flames in order to better understand the soot and thermal radiation emissions of luminous flames. Laminar flames are being studied due to their experimental and computational tractability, noting the relevance of such results to practical turbulent flames through the laminar flamelet concept [1,2]. Weakly-buoyant and nonbuoyant laminar diffusion flames are being considered because buoyancy affects soot processes in flames while most practical flames involve negligible effects of buoyancy [1,2]. Thus, low-pressure weakly-buoyant flames are being observed during ground-based experiments while near-atmospheric pressure nonbuoyant flames will be observed during space flight experiments at microgravity. Finally, premixed laminar flames also are being considered in order to observe some aspects of soot formation for simpler flame conditions than diffusion flames. The present discussion of the investigation is brief, see Refs. 2-20 for more details.

An understanding of soot structure and optical properties is prerequisite to reliable measurements of soot processes in flames; therefore, the initial phases of the investigation emphasized this technology [3-8]. The structure of soot can be seen from the transmission electron microscope (TEM) photograph appearing in Fig. 1. Typical of past observations [21-23], the present soot consists of roughly spherical primary particles having nearly constant diameters at a particular location, collected into aggregates having widely varying numbers of primary particles per aggregate. Aggregates are open structured and can have maximum dimensions up to several μm; therefore, the approximation of Mie scattering for an equivalent sphere is never justified while use of the Rayleigh scattering approximation is questionable [4]. Fortunately, use of the Rayleigh-Debye-Gans scattering approximation for polydisperse populations of fractal aggregates is effective for soot aggregates [4-7], see the comparison between measured and predicted scattering patterns illustrated in Fig. 2. Based on this technology, methods of finding soot volume fraction and soot temperature distributions from laser extinction and multiline emission imaging measurements, needed for both the ground based and the space flight experiments, have been developed [10-13].

Present ground-based experiments involve an extensive suite of measurements to find both soot and flame properties; in contrast, the space flight experiments have limited instrumentation (flame photographs, soot volume fractions and temperatures, soot structure (from TEM) and plume temperatures). As a result, computations of flame structure must be used for properties that are not measured in order to interpret soot processes (velocities and major species concentrations). These predictions are based on the conserved-scalar formalision in conjunction with the laminar-flamelet concept for soot-containing flames [2-4] which circumvents current limitations about fuel decomposition and soot chemistry. This approach involves full numerical simulation of flame structure for axisymmetric steady flow conditions [15-18]. A typical evaluation, involving results along the axis of a weakly-buoyant acetylene/air laminar jet diffusion flame, is illustrated in Fig. 3; the good agreement between predicted and measured velocities, mixture fractions and major species concentrations is evident.

C-5

In view of this status, the main emphasis of current work has been on measurements of soot nucleation and growth in laminar diffusion and premixed flames.

Laminar Diffusion Flames

Introduction. Present ground-based studies of laminar diffusion flames are considering laminar jet diffusion flames similar to the flight experiment. The objectives were to measure both soot and flame properties in hydrocarbon/air laminar jet diffusion flames and to exploit this information to study soot growth and nucleation in diffusion flames.

Experimental Methods. The experiments involved weakly-buoyant round laminar jet-diffusion flames at low pressures, as well as buoyant jet diffusion flames at atmospheric pressure. The following measurements were made: soot volume fractions using laser extinction, gas temperatures using thermocouples where soot is absent and multiline emission where soot is present, soot structure using thermophoretic sampling and analyses by TEM, gas compositions by sampling and analysis with gas chromatography and gas velocities by laser velocimetry.

Results and Discussion. Soot and flame properties along the axis of an acetylene/air flame at 0.25 atm. are illustrated in Fig. 4. Species concentrations for all the flames were in good agreement with generalized state relationships for major gas species [24], adding confidence to the laminar flamelet technique to be used to analyze the flight experiments. Significant levels of soot formation only are observed when temperatures exceed 1250K. The end of soot formation occurs when the concentrations of hydrocarbons become small, at a fuel-equivalence ratio of roughly 1.4. These properties were similar for all the flames [9-12]. The behavior of d_p was more complex, increasing during the early stages of soot formation but reaching a maximum well before the maximum f_s is reached; this behavior is caused by the greater temperature sensitivity of soot nucleation than soot growth so that large nucleation rates toward the end of soot formation yield numerous short residence time primary soot particles, tending to reduce the mean value of d_p.

The measurements were used to study soot growth and nucleation in laminar diffusion flames, inferring growth from the variation of f_s and nucleation from the variation of n_p. It was found that soot growth was reasonably correlated as functions of light hydrocarbon (C_2H_2, C_2H_4, CH_4) concentrations with a low activation energy, and thus best represented as collision efficiencies [9-12]. In addition, acetylene was the dominant light hydrocarbon present in the soot growth region, similar to premixed flames, see Refs. 25-27. It was also important to account for effects of simultaneous soot growth and oxidation due to the presence of soot oxidizing species (H_2O, CO_2 and O_2) within the soot growth region.

The present net soot growth rates, corrected for soot oxidation, are plotted as a function of acetylene concentrations in Fig. 5. The net growth rate has been plotted to anticipate a simple collision efficiency expression. Results shown on the plot involve acetylene/ air diffusion flames (where acetylene is the main hydrocarbon present), other hydrocarbon/air diffusion flames (where C_2H_4 and CH_4 concentrations are comparable to C_2H_2 concentrations) and results from premixed flames from Refs. 25-27. When plotted in this manner, the growth rates for premixed flames exhibit a large vertical span, which is attributed to reduced surface reactivity with age, and growth rates generally lower than the diffusion flames, which may be caused by the uncertain estimates of soot surface areas and residence times for the results of Refs. 25-27. The results for acetylene/air diffusion flames over several studies and a wide range of conditions exhibit first-order behavior with respect to acetylene concentrations which is consistent with a rather reasonable acetylene collision efficiency of 0.39%. In contrast, measurements for other hydrocarbon/air diffusion flames exhibit a consistently higher apparent acetylene collision efficiency of 1.56%; this behavior suggests either parallel soot growth channels through ethylene

collisions (which is present in significant concentrations in these flames), or enhanced surface activation due to the presence of higher hydrogen concentrations in the soot growth region typified by the hydrogen abstraction carbon addition (HACA) mechanism of Mauss et al. [25] and references cited therein.

The rate of formation of primary particles could be associated with the concentration of acetylene in a relatively simple manner. Preliminary examination of the measurements indicated first-order behavior, in agreement with earlier assessments of soot nucleation for various soot formation processes [21, 28]. The resulting soot nucleation rate constant, k_n, is plotted as a function of temperature in Fig. 6, along with an earlier correlation of Leung et al. [28]. The results for all the present hydrocarbon/air flames are in reasonably good agreement with each other (although the scatter is large due to the sensitivity of measured nucleation rates to d_p). The results yield a modest activation energy of 35 kcal/gmol, which is reasonable for a recombination-like process like soot nucleation [21, 28]. Nevertheless, present nucleation rates are significantly lower than the correlation of Leung et al. [28]; this is not surprising because the data used in Ref. 28 involved optical determinations of d_p which are questionable and would tend to overestimate nucleation rates as indicated in Fig. 6 [4].

Laminar Premixed Flames

Introduction. Soot processes in laminar premixed hydrocarbon/air flames have received attention because the flame environment is simpler and more computationally tractable than laminar diffusion flames. Thus, the objective of the present investigation was to apply the techniques developed to study laminar diffusion flames to study soot processes in laminar premixed flames.

Experimental Methods. The measurements were completed using a 60 mm diameter water-cooled porous plug premixed flat flame burner surrounded by a nitrogen shroud flow. The measurements were the same as for the diffusion flames.

Results and Discussion. Measurements of u, d_p, T and f_s are illustrated as a function of height above the burner in Fig. 7. Increased distance from the burner causes increased u due to buoyancy, increased d_p due to growth, decreased T due to radiative heat losses and increased f_s due to soot nucleation and growth. Predictably, larger C/O ratios yield larger soot concentrations and lower temperatures. The measurements of flame and soot structure yield the variations of S, n_p, w_n and w_g illustrated in Fig. 8. Both S and n_p increase with height which implies continued soot nucleation and growth with increasing residence time although both rates decrease similar to past observations [25-27]. This behavior is consistent with the reduced temperatures with increasing distance from the burner exit because both the nucleation rates and the HACA mechanism exhibit temperature dependencies. Quantifying these effects, however, will require information about concentrations of light and heavy hydrocarbons in the flow; current work is carrying out measurements along these lines.

Nomenclature

[i] = molar concentration of species i, d = burner exit diameter, d_p = primary soot particle diameter, C/O = atomic carbon/oxygen ratio, f_s = soot volume fraction, C_{ij}^A = aggregate scattering cross section (i = incident, j = scattered polarization directions), k_n = soot nucleation rate constant, n_p = number of primary particles per unit volume, $\overline{N}$ = mean number of primary particles per aggregate, Re = burner exit Reynolds number, S = soot surface area per unit volume, T = temperature, u = streamwise velocity, $\overline{v}_i$ = mean molecular velocity of species i, w_g = soot growth rate, w_n = soot nucleation rate, X_i = mole fraction of species i, θ = angle of scattering from forward direction.

References

1. Law, C.K. and Faeth, G.M., Prog. Energy Combust. Sci., Vol. 20, 1994, pp. 65-116.
2. Faeth, G. M., *Proceedings of the AIAA/IKI Microgravity Science Symposium*, AIAA, Washington, 1991, pp. 281-293.
3. Köylü, Ü.Ö. and Faeth, G.M., Combust. Flame, Vol. 89, 1992, pp. 140-156.
4. Köylü, Ü.Ö. and Faeth, G.M., J. Heat Trans., Vol. 115, 1993, pp. 409-417.
5. Köylü, Ü.Ö. and Faeth, G.M., J. Heat Trans., Vol. 116, 1994, pp. 152-159.
6. Köylü, Ü.Ö. and Faeth, G.M., J. Heat Trans., Vol. 116, 1994, pp. 971-979.
7. Farias, T.L., Carvalho, M.G., Köylü, Ü.Ö. and Faeth, G.M., J. Heat Trans., Vol. 117, 1995, pp. 152-159.
8. Köylü, Ü.Ö., Faeth, G.M., Farias, T.L. and Carvalho, M.G., Combust. Flame, in press.
9. Sunderland, P.B., Mortazavi, S., Faeth, G.M. and Urban, D.L., Combust. Flame, Vol. 96, 1994, pp. 97-103.
10. Sunderland, P.B., Köylü, Ü.Ö. and Faeth, G.M., Combust. Flame, Vol. 100, 1995, pp. 310-322.
11. Lin, K.-C., Sunderland, P.B. and Faeth, G.M., Combust. Flame, in press.
12. Sunderland, P.B. and Faeth, G.M., Combust. Flame, in press.
13. Faeth, G. M. and Köylü, Ü.Ö., Combust. Sci. Tech., submitted.
14. Lin, K.-C. and Faeth, G.M., J. Prop. Power, submitted.
15. Mortazavi, S., Sunderland, P.B., Jurng, J., Köylü, Ü.Ö. and Faeth, G.M., AIAA Paper No. 93-0708, 1993.
16. Faeth, G.M., Sunderland, P.B., Köylü, Ü.Ö. and Urban, D.L., *Proceedings of International Symposium on Aerospace and Fluid Sciences*, Tohoku University, Sendai, Japan, 1993, pp. 185-198.
17. Köylü, Ü.Ö., Sunderland, P.B., Mortazavi, S. and Faeth, G.M., AIAA Paper No. 94-0428, 1994.
18. Sunderland, P.B. and Faeth, G.M., AIAA Paper No. 95-0149, 1995.
19. Lin, K.-C. and Faeth, G.M., AIAA Paper No. 95-0375, 1995.
20. Xu, F., Sunderland, P.B. and Faeth, G.M., *Proceedings of Spring Technical Meeting*, Canadian Section, The Combustion Institute, Victoria, B.C., in press.
21. Haynes, B. S. and Wagner, H. G., Prog. Energy Combust. Sci., Vol. 7, 1981, pp. 229-273.
22. Glassman, I.,*Twenty-Second Symposium (International) on Combustion*. The Combustion Institute, Pittsburgh, 1988, pp. 295-311.
23. Howard, J.B., *Twenty-Third Symposium (International) on Combustion*, The Combustion Institute, Pittsburgh, 1990, pp. 1107-1127.
24. Sivathanu, Y.R. and Faeth, G.M., Combust. Flame, Vol. 82, 1990, pp. 211-230.
25. Mauss, F., Schäfer, T. and Bockhorn, H., Combust. Flame, Vol. 99, 1995, pp. 697-705.
26. Harris, S.J. and Weiner, A.M., Combust. Sci. Tech., Vol. 38, 1984, pp. 75-87.
27. Ramer, E.R., Merklin, J.F., Sorensen, C.M. and Taylor, T.W., Combust. Sci. Tech., Vol. 48, 1986, pp. 241-255.
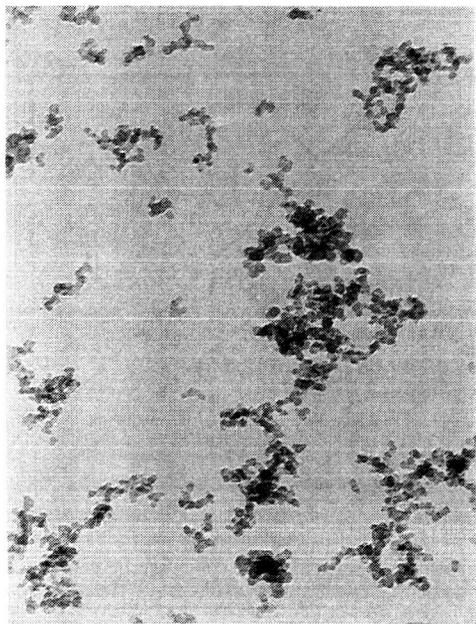28. Leung, K.M., Lindstedt, R.P. and Jones, W.P., Combust. Flame, Vol. 87, 1991, pp. 289-305.

Fig. 1. TEM photograph of soot within a weakly-buoyant acetylene/air laminar jet diffusion flame. Figure dimensions roughly 1000 x 1400 μm.
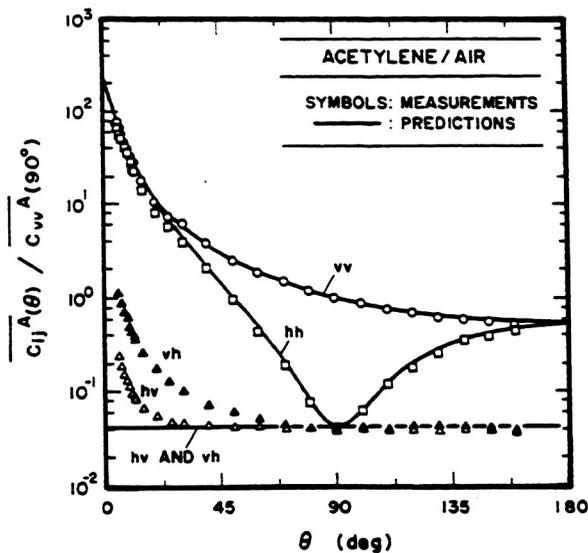

Fig. 2. Scattering pattern for soot emitted from acetylene/air buoyant turbulent diffusion flames. From Köylü and Faeth [5].
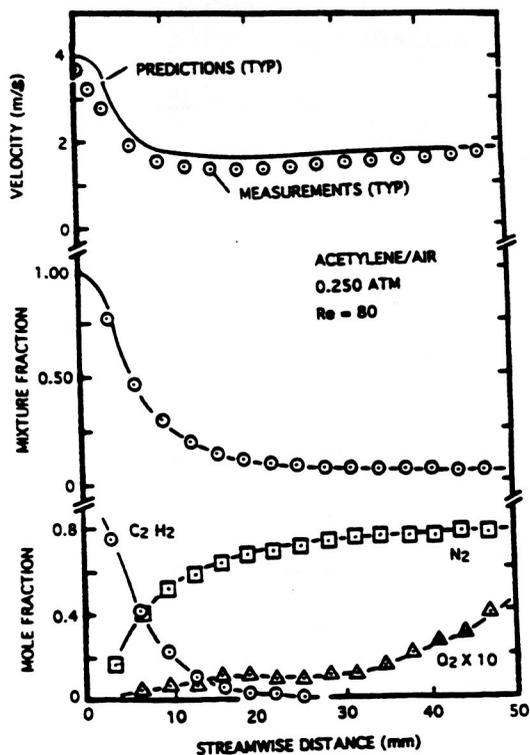

Fig. 3. Measured and predicted properties along the axis of a weakly-buoyant acetylene/air laminar jet diffusion flame. From Köylü et al. [17].
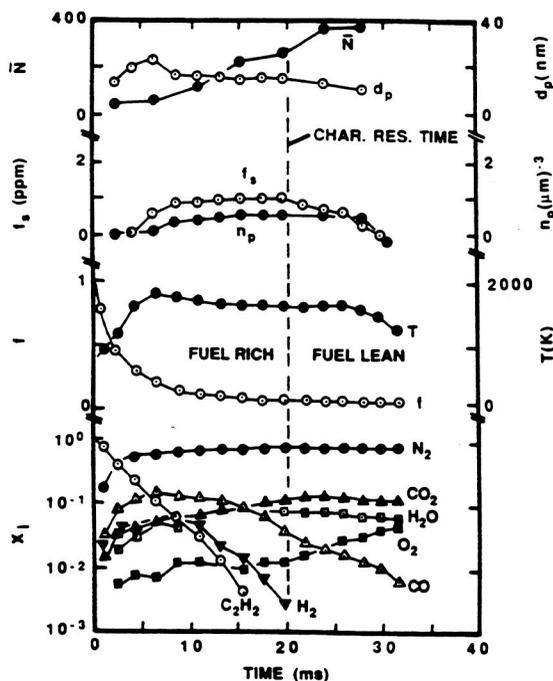

Fig. 4. Soot and flame properties along the axis of a weakly-buoyant acetylene/air laminar jet diffusion flame at 0.25 atm. From Sunderland et al. [10].
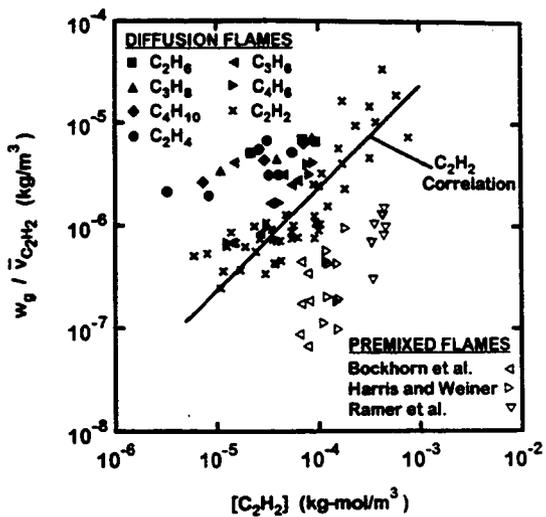
Fig. 5. Net soot growth rates after connection for oxidation within laminar hydrocarbon/air jet diffusion flames. From Sunderland and Faeth [12].
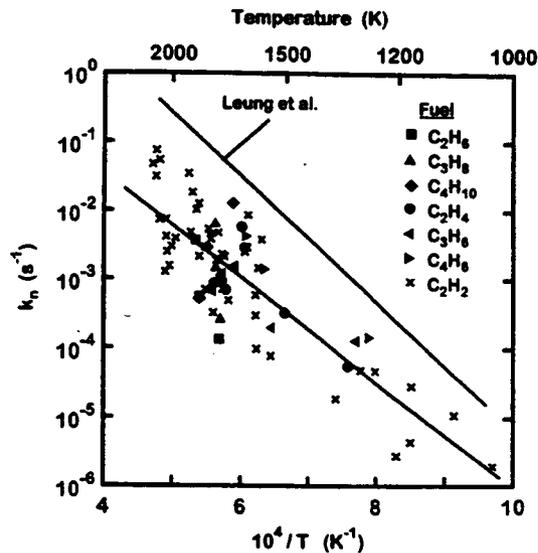
Fig. 6. Soot nucleation rates within laminar hydrocarbon/air jet diffusion flames. From Sunderland and Faeth [12].
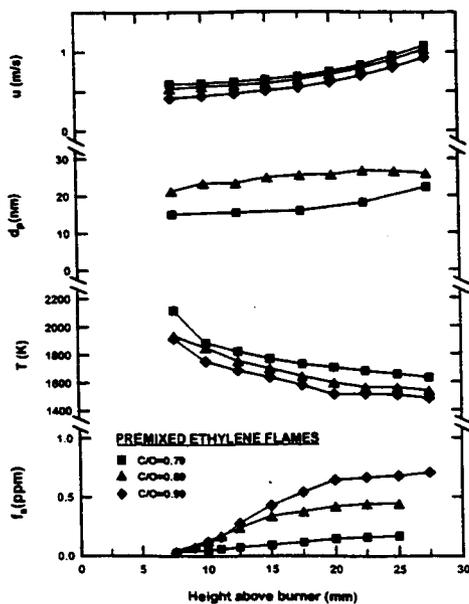
Fig. 7. Measured flame and soot properties along the axis of premixed laminar ethylene/air flames at atmospheric pressure. From Xu et al. [20].
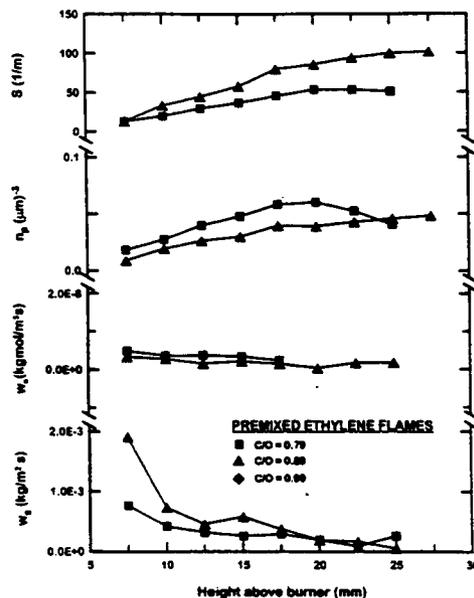
Fig. 8. Derived soot properties along the axis of premixed ethylene/air flames at atmospheric pressure. From Xu et al. [20].